

**Hybrid gold nanoparticle-reduced graphene oxide nanosheets as active catalysts for highly efficient reduction of nitroarenes†**Yuri Choi,<sup>a</sup> Hee Son Bae,<sup>b</sup> Eunyong Seo,<sup>a</sup> Seonwan Jang,<sup>b</sup> Kang Hyun Park<sup>\*b</sup> and Byeong-Su Kim<sup>\*a</sup>

Received 1st June 2011, Accepted 19th July 2011

DOI: 10.1039/c1jm12477c

We demonstrate a simple, one-step synthesis of hybrid gold nanoparticle–graphene oxide nanosheets (Au–GO) through electrostatic self-assembly. This method affords a facile means of controlling the effective concentration of the active Au nanoparticles on the graphene sheets, but also offers the necessary stability of the resulting Au–GO nanostructure for catalytic transformation. Furthermore, this hybrid Au–GO is successfully employed in the catalytic reduction of a series of nitroarenes with high catalytic activity. Through careful investigation of the catalyst, we find the synergistic catalytic effect of Au nanoparticles and GO, further highlighting the significance of hybrid Au–GO nanostructure. Considering the wide potential applications of a two-dimensional graphene sheet as a host material for a variety of nanoparticles, the approach developed here may lead to new possibilities for the fabrication of hybrid nanoparticle–graphene nanosheet structures endowed with multiple functionalities.

**Introduction**

Graphene, a monolayer of aromatic carbon lattice, has attracted considerable interest in recent years in many fields of science and engineering.<sup>1</sup> This interest can be attributed to the extraordinary electrical, optical, thermal, and mechanical properties of graphene and its related carbon nanostructures.<sup>2–5</sup> While earlier synthetic methods for graphene production were challenging, there have been considerable advancements in the synthesis and processing methods, such as micromechanical exfoliation, oxidation/reduction protocols, epitaxial growth, and vapor deposition.<sup>6–8</sup> These improved methods have enabled the realization of graphene-based materials for applications to nanotechnology.<sup>9–12</sup> Among various types of graphene and related carbon nanostructures, a stable suspension of graphene oxide (GO) is the common choice over pristine graphene owing to its facile synthetic nature in a controlled, scalable, and reproducible manner.<sup>7,13,14</sup> The abundant oxygen-containing functional groups such as epoxide, alcohol, and carboxylic acids provide GO with excellent aqueous dispersity and also offer anchors for further chemical modifications. Taking full advantage of the surface

functional groups, together with its large specific surface area, GO nanosheets are emerging as promising supports for the creation of hybrid nanomaterials and, in particular, in catalytic applications.<sup>15</sup> To date, a variety of metal, metal oxide, semiconducting, and magnetic nanoparticles (NPs) including Pd,<sup>16–18</sup> Pt,<sup>19–22</sup> Au,<sup>23–26</sup> TiO<sub>2</sub>,<sup>27–30</sup> and Fe<sub>3</sub>O<sub>4</sub><sup>31</sup> have been hosted on the surface of GO. Many of these hybrid nanocomposites find applications as electrocatalysts; however, few papers thus far have reported on the utilization of metal NPs anchored to graphene and on their catalytic activity for organic transformation.<sup>16,32</sup> For example, Mulhaupt and co-workers have reported on the catalytic activity of Pd NPs supported on GO for the Suzuki–Miyaura coupling reaction.<sup>16</sup>

In this article, we present a simple and facile approach for integrating gold (Au) NPs onto the surface of graphene nanosheets by electrostatic self-assembly. This method not only provides a facile means of controlling the effective concentration of the active Au NPs, but also offers the necessary stability of the resulting nanocomposite for catalytic transformation. Furthermore, we exploit that the resulting hybrid Au NP–GO nanosheets exhibit excellent catalytic activity toward the reduction of a series of model nitroarenes (Fig. 1). Beyond our expectation and to our surprise, we find that the graphene nanosheet is not only presenting a high surface area as a catalytic support for Au NPs, but also accelerating the reaction by itself with its unique electronic structures of graphene edges; thus synergistically facilitating the catalytic activity toward the reduction of model nitroarenes. For their mature synthetic protocols and good catalytic properties, here we choose the Au NPs, but this method can be easily extended to other NPs with sufficient surface charge. Considering the wide-ranging potential applications of

<sup>a</sup>Interdisciplinary School of Green Energy and School of NanoBioscience and Chemical Engineering, UNIST (Ulsan National Institute of Science and Technology), Ulsan, 689-798, Korea. E-mail: bskim19@unist.ac.kr; Fax: +82-52-217-2909; Tel: +82-52-217-2923

<sup>b</sup>Department of Chemistry and Chemistry Institute for Functional Materials, Pusan National University, Busan, 609-735, Korea. E-mail: chemistry@pusan.ac.kr; Fax: +82-51-980-5200; Tel: +82-51-510-2238

† Electronic supplementary information (ESI) available: Additional characterization data of fluorescence quenching, elemental analysis, TEM and additional catalytic conversion data. See DOI: 10.1039/c1jm12477c

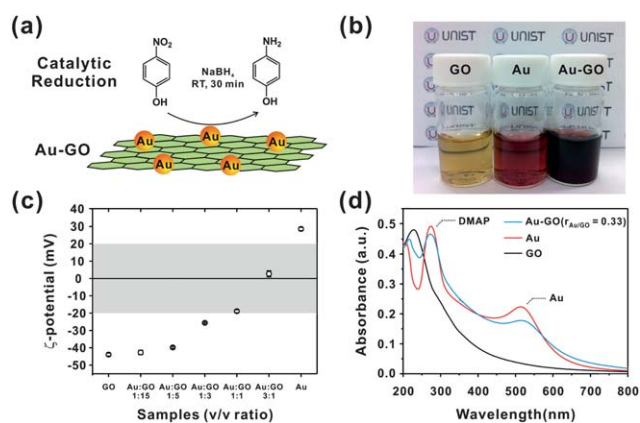


**Fig. 1** (a) Schematic illustration of electrostatic self-assembly of Au nanoparticles on GO nanosheets and their catalytic applications. (b) The corresponding images of suspensions of (left) GO, (middle) Au NPs, and (right) hybrid Au-GO ( $r_{\text{Au/GO}} = 0.33$ ). (c)  $\zeta$ -Potential and (d) UV/vis spectra of hybrid Au-GO with different volume ratios of each component. All values are the average of three individual measurements with a standard deviation as an error bar.

a two-dimensional graphene sheet as a host material for a variety of NPs, the approach developed here may lead to new possibilities for the fabrication of hybrid NP-GO structures endowed with multiple functionalities.

## Experimental

### Preparation of DMAP-Au nanoparticles

The DMAP-Au nanoparticles were prepared according to a literature method.<sup>35</sup> In brief, 30 mM aqueous metal chloride solution ( $\text{HAuCl}_4 \cdot 3\text{H}_2\text{O}$ , 30 mL) was added to a 25 mM solution of tetraoctylammonium bromide in toluene (80 mL). A 0.40 M solution of freshly prepared  $\text{NaBH}_4$  (25 mL) was added to the stirred mixture, which caused an immediate reduction to occur. After 30 min, the two phases were separated and the toluene phase was subsequently washed with 0.10 M  $\text{H}_2\text{SO}_4$ , 0.10 M  $\text{NaOH}$ , and  $\text{H}_2\text{O}$  (three times), and then dried over anhydrous  $\text{Na}_2\text{SO}_4$ . An aqueous 4-dimethylaminopyridine (DMAP) solution (0.10 M, 1.0 mL) was added to aliquots (1.0 mL) of the as-prepared nanoparticle mixtures. This concentration of DMAP was found to be sufficient to affect the complete and spontaneous phase transfer of the nanoparticles. Direct phase transfer across the organic/aqueous boundary was completed within 1 h without additional stirring.

### Preparation of GO and hybrid Au-GO nanocomposites

Graphite oxide was synthesized from graphite powder (Aldrich) by modified Hummers method and exfoliated to give a brown dispersion of graphene oxide (GO) under ultrasonication. The resulting GO suspension (15 mL,  $0.50 \text{ mg mL}^{-1}$ ) was mixed with 5.0 mL of DMAP-Au nanoparticles (1 : 3 v/v ratio vs. GO,  $r_{\text{Au/GO}} = 0.33$ ), followed by stirring at room temperature for 3 h. Then, the resulting mixture was centrifuged and thoroughly washed with ethanol and deionized water (3 times) to remove free Au nanoparticles. Finally, the precipitate was redispersed in

5.0 mL of water. In addition, the amount of NPs was controlled by changing the volume ratio (v/v ratio of DMAP-Au : GO) from 3 : 1, 1 : 1, 1 : 3, 1 : 5, to 1 : 15.

### Catalytic reduction of 4-nitrophenol by hybrid Au-GO nanocomposites

As a representative example, 0.25 mL of  $1.49 \times 10^{-4} \text{ M}$  (0.50 mol% with respect to the gold concentration) Au-GO ( $r_{\text{Au/GO}} = 0.33$ ) was mixed with 1.0 mL of 2.22 M  $\text{NaBH}_4$  (300 equiv. to the substrate, >97%, TCI) solution, and the mixture was sonicated for 1 min at room temperature. Then, 10 mL of  $7.50 \times 10^{-4} \text{ M}$  4-nitrophenol (>99%, Aldrich) was added to the mixture and was allowed to stir until the deep yellow solution became colorless. The yellow color of the solution gradually vanished, indicating the reduction of 4-nitrophenol. The reaction progress was checked by assessing a small portion of the reaction mixture at a regular time interval (5 min). The concentration of 4-nitrophenol was determined spectrophotometrically at a wavelength of 400 nm using a SINCO S-3150 spectrophotometer.

### Characterizations

The  $\zeta$ -potential of colloidal suspensions at pH 6–8 was measured using a zeta potential analyzer (Malvern, Zetasizer nano-zs). The surface morphology of the samples was investigated using atomic force microscopy (AFM, Nanoscope V, Veeco) *via* a tapping mode and energy-filtering transmission electron microscope (TEM, Carl Zeiss-LIBRA 120). The composition of each component within the hybrid Au-GO was measured by using a thermogravimetric analyzer (TGA, TA Instrument). The fluorescence emission spectra of the hybrid solution were recorded by a fluorometer (Varian). An element analyzer (Thermo Scientific) determined the weight percentages of carbon, hydrogen, nitrogen, and oxygen of the hybrid Au-GO.

## Results and discussion

The GO suspension was initially prepared according to the modified Hummers method from a commercially available graphite powder.<sup>33,34</sup> Following sonication for exfoliation of graphite oxide, the chemical functional groups introduced on the surface of the graphene sheet such as carboxylic acids ( $\text{COOH}$ ) render the prepared GO suspension negatively charged over a wide range of pH conditions ( $\text{GO-COO}^-$ ). The resulting  $\text{GO-COO}^-$  nanosheets exhibit a fairly good colloidal stability with a  $\zeta$ -potential of  $-44 \pm 0.9 \text{ mV}$  (Fig. 1c). The as-prepared colloidal suspension of GO mainly comprises single-layer graphene nanosheets having a thickness of approximately 0.70 nm with lateral dimensions of 0.70–1.5  $\mu\text{m}$ , as determined by atomic force microscopy (AFM). The positively charged Au NPs were prepared based on the spontaneous phase transfer of organic soluble Au NPs across the aqueous phase using 4-dimethylaminopyridine (DMAP), a readily available organic ligand that ensures the monodispersity of the NPs and affords the necessary stability in an aqueous solvent.<sup>35</sup> The resulting DMAP-coated Au NPs have an average diameter of 6 nm with a high surface potential of +35 mV. Once the two oppositely charged nanostructures are synthesized, they are coupled to form a stable hybrid nanocomposite based on the electrostatic self-assembly

between positively charged DMAP–Au NPs and negatively charged GO–COO<sup>−</sup> nanosheets. As soon as the Au NPs are added to the GO suspension, a mild surface-charge-driven precipitate appears. The solution is subjected to successive cycles of centrifugation to remove unbound free Au NPs, and the solution is then redispersed in water. The obtained black homogeneous aqueous dispersion remains stable without any noticeable aggregates for several months (Fig. 1b).

While varying the relative ratio of Au NPs to GO (hereafter,  $r_{\text{Au/GO}}$ ) at a fixed amount of GO, we found that there is an optimum ratio between the Au NPs and GO that is required to provide the necessary aqueous stability to hybrid Au–GO. The  $\zeta$ -potential increases from  $-44 \pm 0.9$  mV (pure GO) to  $-26 \pm 0.4$  mV ( $r_{\text{Au/GO}} = 0.33$ ). Furthermore, the  $\zeta$ -potential even reversed to  $+2.7 \pm 1.8$  mV in the presence of excess Au NPs ( $r_{\text{Au/GO}} = 3$ ) which do not readily redisperse in water due to aggregation at this ratio (Fig. 1a). Consequently, for catalytic applications, here we choose  $r_{\text{Au/GO}} = 0.33$ , thus ensuring the stability of the composite during the reaction in aqueous media. UV/vis spectroscopy further supports that the surface plasmon resonance peak of starting Au NPs ( $\lambda_{\text{max}} = 514$  nm) is not altered significantly after the formation of hybrid Au–GO ( $\lambda_{\text{max}} = 526$  nm) (Fig. 1d). It is also of note that the peak from DMAP is observed in the spectra of Au–GO hybrid.

Fig. 2 illustrates the typical transmission electron microscopy (TEM) and AFM images of the hybrid composite prepared from the hybrid Au–GO ( $r_{\text{Au/GO}} = 0.33$ ). The graphene sheets are covered with a high density of Au NPs as shown in all images. Interestingly, we found that the edges of graphene sheets as well as the basal planes are covered with Au NPs, although the densities are still relatively higher at the edges due to the higher distribution of surface functional groups at the edges (ESI†); however, given the strong interaction between Au NPs even with basal plane as observed in the TEM, we could not exclude the contribution arising from other intermolecular interactions such

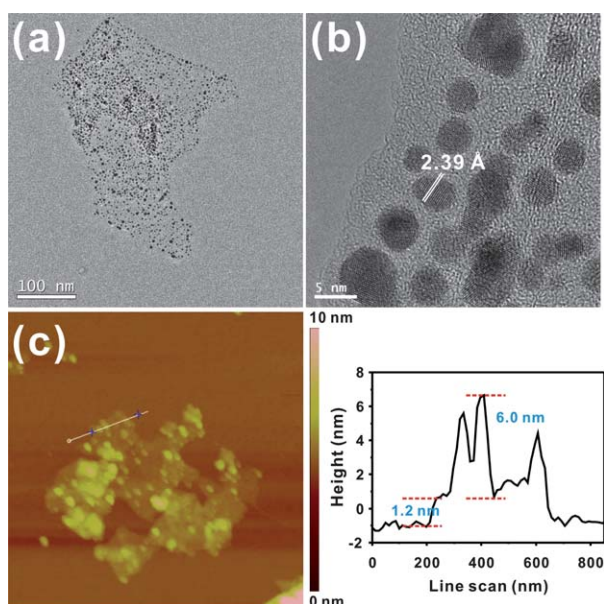


**Fig. 2** (a and b) TEM and (c) AFM images of hybrid Au–GO with a corresponding line scan profile. The scale is  $5 \mu\text{m} \times 5 \mu\text{m}$  in (c).

as the  $\pi$ – $\pi$  interactions between the residual  $\pi$ -conjugated domains in GO and the aromatic surface stabilizer of Au NPs, namely, DMAP. HR-TEM reveals the highly crystalline nature of Au NPs with a lattice spacing of 2.39 Å, as has been reported in the literature.<sup>35</sup> In addition, the AFM image supports the self-assembled structure of hybrid Au–GO. We found that the GO sheets bearing NPs are more corrugated as compared to the initial state of the GO before the assembly. The AFM line scan also represents that the individual Au NPs of approximately 6.0 nm in diameter are deposited onto the surface of functionalized GO with a height of 1.2 nm.

Independent of these observations, the Au NPs anchored on the surface of graphene nanosheets effectively quench the intrinsic fluorescence of the GO nanosheets, thus serving to further highlight the strong interactions between the two components (ESI†).<sup>36</sup> Thermogravimetric analysis (TGA) was employed to determine the relative composition of each component within hybrid Au–GO (Fig. 3). As shown in the TGA curve, initial mass loss of water followed by the rapid decomposition of hybrid Au–GO is observed from the decomposition of labile oxygen-containing surface functional groups on GO. The relative composition can be determined from the final decomposed product, which suggests that approximately 62% Au NPs are contained in the hybrid Au–GO ( $r_{\text{Au/GO}} = 0.33$ ). Other hybrid Au–GO structures with varying composition ratios exhibit a similar trend of relative ratio of Au NPs with respect to the GO (Fig. 3).

After the careful investigation of the hybrid Au–GO nanocomposites prepared, it was employed in the catalytic reduction of a series of nitroarenes in the presence of NaBH<sub>4</sub> as a hydrogen source, because Au NPs are well known to be effective in the conversion of nitroarenes. Nitroarenes are typically found in industrial products and agricultural waste waters and known to be harmful and hazardous. As such, there are various physical, biological, and chemical methods such as adsorption, microbial degradation, and electrochemical treatment as well as catalytic reactions developed for the removal of nitroarenes. Among them, selective hydrogenation of nitroarenes to the corresponding aminoarenes is known as one of the fundamental reactions

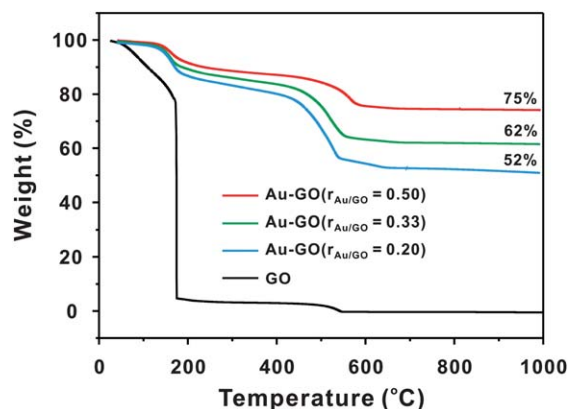


**Fig. 3** TGA thermograms of the hybrid Au–GO nanocomposites with a varying ratio of each component. The thermograms were obtained at a scan rate of  $10 \text{ }^\circ\text{C min}^{-1}$  under air. The relative composition of Au NPs within the hybrid Au–GO is represented in each scan.

for the synthesis and manufacture of fine and industrial chemicals for the production of pharmaceutical and agrochemical products, dyes, rubbers, and polymers.

To evaluate the catalytic activity of hybrid Au–GO, we first tested the reduction of 4-nitrophenol with hybrid Au–GO ( $r_{\text{Au/GO}} = 0.33$ ). As shown in Fig. 4a, the UV/vis spectra of the reaction mixture were monitored with the progress of the catalytic reduction of 4-nitrophenol. Specifically, the absorption of 4-nitrophenol at 400 nm decreases rapidly with a concomitant increase in the peak at 300 nm, which is attributed to the reduced product, 4-aminophenol. The isosbestic point between the two peaks is also observed, suggesting that the two principal species are responsible for the reaction conversion. From the UV/vis spectra, therefore, the pseudo-first-order reaction kinetics was applied to determine the reaction rate constant. From the linear relations of  $\ln(C_t/C_0)$ , shown in Fig. 4b, we found that the rate constant,  $k$ , for this reaction is  $0.124 \text{ min}^{-1}$ , which is comparable to those reported previously (typical values are approximately  $10^{-1}$  to  $10^{-3} \text{ min}^{-1}$ ).<sup>37</sup>

The control experiments further elucidated the reaction mechanism of hybrid Au–GO catalyst for the reduction of nitroarenes. To our surprise, the control experiment wherein GO is used exclusively in the above reaction yielded appreciable reduction of the reactant albeit at much lower efficiency under the reaction condition tested initially (5.0 mol% of catalyst, 50 equiv. of  $\text{NaBH}_4$  to substrate). However, most notably when the amount of  $\text{NaBH}_4$  is increased considerably (300 equiv. to substrate), the reaction proceeds in a highly effective manner compared to 50 equiv. of  $\text{NaBH}_4$ , and it is also proved to occur well even in the absence of Au NPs. We then investigated to optimize the amount of catalyst as well as the amount of the  $\text{NaBH}_4$  introduced during the reduction. After careful examinations, we found that not only the Au NPs, but also GO at its reduced state, which are commonly referred to as a reduced graphene oxide (rGO), is playing a key role in enhancing the catalytic efficiency of the reaction. Because  $\text{NaBH}_4$  is commonly used to reduce GO to rGO,<sup>38</sup> the added reductant  $\text{NaBH}_4$  in the reduction of nitroarenes can simultaneously reduce the GO, and the resulting rGO can be responsible for the observed catalytic activity. In concert with our observation, Bao and co-workers have recently reported that rGO is capable of reducing nitroarenes with high efficiency at room temperature.<sup>39</sup> Based on the DFT calculation, they attributed this catalytic activity of rGO to the unique electronic structure of the zigzag edges of graphene, which interact with the terminal oxygen atoms of nitrophenol

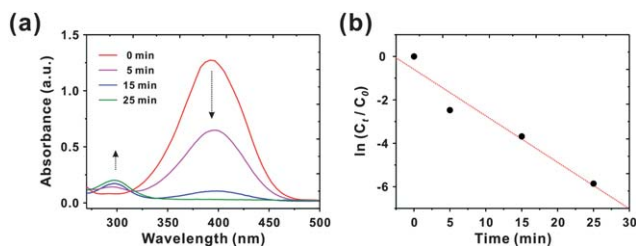


**Fig. 4** (a) Time-dependent UV/vis absorption spectra for the reduction of 4-nitrophenol over hybrid Au–GO catalyst in aqueous media at 298 K. (b) Plot of  $\ln(C_t/C_0)$  versus time for the reduction of 4-nitrophenol. 5.0 mol% of catalyst and 50 equiv. of  $\text{NaBH}_4$  are used for the reaction.

derivatives, hence weakening the N–O bonds for effective reduction to occur. This is an interesting observation using carbon material exclusively as a catalyst for organic transformation; nevertheless, it should be pointed out that our hybrid Au–GO still exhibits better catalytic activity relative to Au NP and GO nanosheets in all cases alone on account of the combined, synergistic catalytic effects of each component (Fig. 5). As shown in the Fig. 5d, when the reaction rate constant,  $k$ , of each catalyst is compared, the Au–GO hybrid shows a strikingly higher catalytic efficiency ( $6.478 \text{ min}^{-1}$ ) than that from the respective catalyst, Au ( $0.069 \text{ min}^{-1}$ ) and GO ( $0.038 \text{ min}^{-1}$ ) (note the sum of rate constant from each Au and GO is significantly smaller than that of Au–GO hybrid). Other experiments under different reaction conditions all produced the identical results of increased catalytic activity in the hybrid Au–GO catalyst compared to individual component (Fig. 5e). It is worth mentioning that the catalytic efficiency of GO is relatively higher at low catalyst content, whereas the catalytic efficiency of Au NPs becomes higher at high content of catalyst used. On the other hand, the catalytic efficiency of GO tends to increase upon addition of more  $\text{NaBH}_4$  in all cases, which supports the key role of rGO in this reaction. We postulate that such increased catalytic activity of hybrid Au–GO is attributable to two factors: GO nanosheet that can promote the adsorption of reactants and

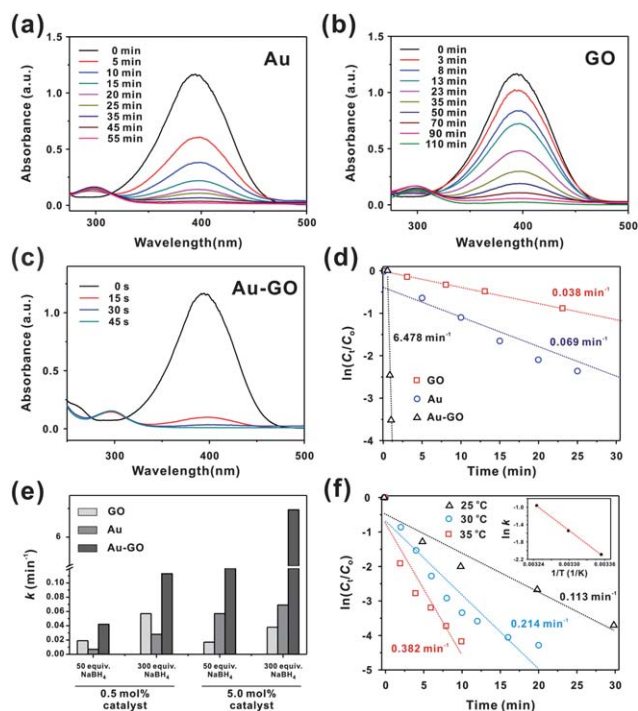


**Fig. 5** (a–c) Time-dependent UV/vis absorption spectra for the reduction of 4-nitrophenol over (a) Au, (b) GO, and (c) Au–GO catalyst in aqueous media at 298 K. (d) Plot of  $\ln(C_t/C_0)$  versus time for the reduction of 4-nitrophenol with different catalysts. All catalysts are used at the same molar ratio of 5.0 mol% of catalyst and 300 equiv. of  $\text{NaBH}_4$  for the reaction. (e) Comparison of reaction rate constants of all catalysts in this study. (f) Plot of  $\ln(C_t/C_0)$  versus time and (inset) the corresponding Arrhenius plot for the reduction of 4-nitrophenol over hybrid Au–GO catalysts under different temperatures at 0.50 mol% of catalyst and 300 equiv. of  $\text{NaBH}_4$ .

facilitate the reaction kinetics with its free electrons on the surface and the additional stability of catalytic Au NPs supported by the graphene nanosheet that prevent the aggregation of NPs, which are common issues in using NP catalyst in organic transformation.

We have further investigated the catalytic activity of hybrid Au–GO for the reduction of other nitroarene analogues (Table 1). Here, we choose to run the reactions in the presence of 0.50 mol% of catalyst with 300 equiv. of NaBH<sub>4</sub> to clearly monitor the conversion efficiency of the reaction. As shown in Table 1, we found that our Au–GO hybrid exhibits high reactivity with excellent yields toward a series of model nitrophenols and anilines compounds regardless of the types and position of the substituents. For example, the Au–GO catalysts led to complete conversion of 4-aminophenol within 30 min (Table 1, entry 1). Interestingly, when the reduction of 4-, 3-, and 2-nitrophenols was catalyzed by Au–GO nanosheet, the 3- and 2-nitrophenols showed a better activity than that of 4-nitrophenol. Remarkably, the turnover frequency (TOF) in entry 2 is 2400 s<sup>-1</sup>, calculated by the moles of nitroarene consumed per mole of the hybrid Au–GO catalyst per 1 s under the present reaction condition. To the best of our knowledge, this is the highest activity of reduction of nitroarenes using Au NPs reported to date. Once again, this result highlights the utility of our hybrid Au–GO catalyst by the synergistic catalytic effect of Au NPs and GO nanosheet. As

shown in the second series of experiments performed with various nitroanilines, the hybrid Au–GO still exhibits good catalytic activity. It is also interesting to note that the 3-nitroaniline displays better conversion efficiency than other analogues, as similarly observed with the nitrophenols.

Finally, we have conducted identical reactions at various temperatures and observed the subtle increase in temperature has a significant impact on the reaction rate constants. The obtained rate constants were plotted to provide the activation energy of the reaction, which corresponds to approximately 85.9 kJ mol<sup>-1</sup> by deducing the Arrhenius plot (Fig. 5f).

## Conclusion

In conclusion, we have developed a simple, one-step synthesis of hybrid gold (Au) nanoparticles–graphene oxide (GO) nanosheets based on the electrostatic self-assembly of two oppositely charged suspensions of Au nanoparticles with GO nanosheets. This method affords a facile means of controlling the effective concentration of the active Au nanoparticles on the graphene sheets, but also offers the necessary stability of the resulting Au–GO nanostructure for catalytic transformation. The prepared hybrid Au–GO is successfully employed in the catalytic reduction of a series of nitroarenes with a high catalytic activity by the synergistic catalytic effect of Au nanoparticles and GO, further highlighting the importance of hybrid Au–GO nanostructure. Although the high catalytic activity of nitrogen-doped graphene and related carbon nanostructures is already well-recognized as effective electrocatalysts in fuel cells,<sup>40–43</sup> the application of rGO in the organic transformation is still in its infancy. Considering the wide potential applications of a two-dimensional graphene sheet as a host material for a variety of nanoparticles, the approach developed here may lead to new possibilities for integrating active nanoparticles with graphene nanosheets for advanced electronic, energy, and catalytic applications.

## Acknowledgements

This research was supported by WCU (World Class University) program through the Korea Science and Engineering Foundation funded by the Ministry of Education, Science and Technology (R31-2008-000-20012-0) and by Basic Science Research Program through the National Research Foundation of Korea (NRF) funded by the Ministry of Education, Science and Technology (2009-0070926, 2010-0002834, 2010-0029434).

## Notes and References

- 1 K. S. Novoselov, A. K. Geim, S. V. Morozov, D. Jiang, Y. Zhang, S. V. Dubonos, I. V. Grigorieva and A. A. Firsov, *Science*, 2004, **306**, 666–669.
- 2 S. Stankovich, D. A. Dikin, G. H. B. Dommett, K. M. Kohlhaas, E. J. Zimney, E. A. Stach, R. D. Piner, S. T. Nguyen and R. S. Ruoff, *Nature*, 2006, **442**, 282–286.
- 3 A. A. Balandin, S. Ghosh, W. Z. Bao, I. Calizo, D. Teweldebrhan, F. Miao and C. N. Lau, *Nano Lett.*, 2008, **8**, 902–907.
- 4 Z. Lee, K. J. Jeon, A. Dato, R. Erni, T. J. Richardson, M. Frenklach and V. Radmilovic, *Nano Lett.*, 2009, **9**, 3365–3369.
- 5 K. P. Loh, Q. L. Bao, G. Eda and M. Chhowalla, *Nat. Chem.*, 2010, **2**, 1015–1024.
- 6 K. S. Novoselov, D. Jiang, F. Schedin, T. J. Booth, V. V. Khotkevich, S. V. Morozov and A. K. Geim, *Proc. Natl. Acad. Sci. U. S. A.*, 2005, **102**, 10451–10453.

**Table 1** Reduction of various nitroarenes using hybrid Au–GO catalyst<sup>a</sup>

Entry	Substrate	Product	Time/min	TOF/s <sup>-1</sup>
1			30	400
2			5	2400
3			6	2000
4			40	300
5			10	1200
6			14	857

<sup>a</sup> Reaction condition: 10 mL of 7.50 × 10<sup>-4</sup> M nitroarene, 0.25 mL of 1.49 × 10<sup>-4</sup> M hybrid Au–GO (0.50 mol% with respect to the gold concentration), 1.0 mL of 2.22 M NaBH<sub>4</sub> (300 equiv. to the substrate).

- 7 G. Eda, G. Fanchini and M. Chhowalla, *Nat. Nanotechnol.*, 2008, **3**, 270–274.
- 8 K. S. Kim, Y. Zhao, H. Jang, S. Y. Lee, J. M. Kim, J. H. Ahn, P. Kim, J. Y. Choi and B. H. Hong, *Nature*, 2009, **457**, 706–710.
- 9 D. A. Dikin, S. Stankovich, E. J. Zimney, R. D. Piner, G. H. B. Dommett, G. Evmenenko, S. T. Nguyen and R. S. Ruoff, *Nature*, 2007, **448**, 457–460.
- 10 X. L. Li, G. Y. Zhang, X. D. Bai, X. M. Sun, X. R. Wang, E. Wang and H. J. Dai, *Nat. Nanotechnol.*, 2008, **3**, 538–542.
- 11 J. Balapanuru, J. X. Yang, S. Xiao, Q. L. Bao, M. Jahan, L. Polavarapu, J. Wei, Q. H. Xu and K. P. Loh, *Angew. Chem., Int. Ed.*, 2010, **49**, 6549–6553.
- 12 Y. Li, Y. Hu, Y. Zhao, G. Q. Shi, L. E. Deng, Y. B. Hou and L. T. Qu, *Adv. Mater.*, 2011, **23**, 776–780.
- 13 D. Li, M. B. Muller, S. Gilje, R. B. Kaner and G. G. Wallace, *Nat. Nanotechnol.*, 2008, **3**, 101–105.
- 14 S. Park and R. S. Ruoff, *Nat. Nanotechnol.*, 2009, **4**, 217–224.
- 15 P. V. Kamat, *J. Phys. Chem. Lett.*, 2011, **2**, 242–251.
- 16 G. M. Scheuermann, L. Rumi, P. Steurer, W. Bannwarth and R. Mulhaupt, *J. Am. Chem. Soc.*, 2009, **131**, 8262–8270.
- 17 S. J. Guo, S. J. Dong and E. W. Wang, *ACS Nano*, 2010, **4**, 547–555.
- 18 J. Yang, C. Tian, L. Wang and H. Fu, *J. Mater. Chem.*, 2011, **21**, 3384–3390.
- 19 E. Yoo, T. Okata, T. Akita, M. Kohyama, J. Nakamura and I. Honma, *Nano Lett.*, 2009, **9**, 2255–2259.
- 20 Y. G. Zhou, J. J. Chen, F. B. Wang, Z. H. Sheng and X. H. Xia, *Chem. Commun.*, 2010, **46**, 5951–5953.
- 21 S. J. Guo, D. Wen, Y. M. Zhai, S. J. Dong and E. K. Wang, *ACS Nano*, 2010, **4**, 3959–3968.
- 22 S. Zhang, Y. Y. Shao, H. G. Liao, M. H. Engelhard, G. P. Yin and Y. H. Lin, *ACS Nano*, 2011, **5**, 1785–1791.
- 23 R. Muszynski, B. Seger and P. V. Kamat, *J. Phys. Chem. C*, 2008, **112**, 5263–5266.
- 24 Y. Fang, S. Guo, C. Zhu, Y. Zhai and E. Wang, *Langmuir*, 2010, **26**, 11277–11282.
- 25 W. J. Hong, H. Bai, Y. X. Xu, Z. Y. Yao, Z. Z. Gu and G. Q. Shi, *J. Phys. Chem. C*, 2010, **114**, 1822–1826.
- 26 Y. Wang, S. Zhang, D. Du, Y. Shao, Z. Li, J. Wang, M. H. Engelhard, J. Li and Y. Lin, *J. Mater. Chem.*, 2011, **21**, 5319–5325.
- 27 Y. S. Hu, L. Kienle, Y. G. Guo and J. Maier, *Adv. Mater.*, 2006, **18**, 1421–1426.
- 28 D. H. Wang, D. W. Choi, J. Li, Z. G. Yang, Z. M. Nie, R. Kou, D. H. Hu, C. M. Wang, L. V. Saraf, J. G. Zhang, I. A. Aksay and J. Liu, *ACS Nano*, 2009, **3**, 907–914.
- 29 X. Y. Zhang, H. P. Li, X. L. Cui and Y. H. Lin, *J. Mater. Chem.*, 2010, **20**, 2801–2806.
- 30 K. K. Manga, S. Wang, M. Jaiswal, Q. L. Bao and K. P. Loh, *Adv. Mater.*, 2010, **22**, 5265–5270.
- 31 B. Li, H. Cao, J. Shao, M. Qu and J. H. Warner, *J. Mater. Chem.*, 2011, **21**, 5069–5075.
- 32 Z. H. Tang, S. L. Shen, J. Zhuang and X. Wang, *Angew. Chem., Int. Ed.*, 2010, **49**, 4603–4607.
- 33 W. S. Hummers and R. E. Offeman, *J. Am. Chem. Soc.*, 1958, **80**, 1339.
- 34 T. K. Hong, D. W. Lee, H. J. Choi, H. S. Shin and B. S. Kim, *ACS Nano*, 2010, **4**, 3861–3868.
- 35 D. I. Gittins and F. Caruso, *Angew. Chem., Int. Ed.*, 2001, **40**, 3001–3004.
- 36 J. H. Jung, D. S. Cheon, F. Liu, K. B. Lee and T. S. Seo, *Angew. Chem., Int. Ed.*, 2010, **49**, 5708–5711.
- 37 J. Lee, J. C. Park and H. Song, *Adv. Mater.*, 2008, **20**, 1523–1528.
- 38 H. J. Shin, K. K. Kim, A. Benayad, S. M. Yoon, H. K. Park, I. S. Jung, M. H. Jin, H. K. Jeong, J. M. Kim, J. Y. Choi and Y. H. Lee, *Adv. Funct. Mater.*, 2009, **19**, 1987–1992.
- 39 Y. J. Gao, D. Ma, C. L. Wang, J. Guan and X. H. Bao, *Chem. Commun.*, 2011, **47**, 2432–2434.
- 40 L. Qu, Y. Liu, J. B. Baek and L. Dai, *ACS Nano*, 2010, **4**, 1321–1326.
- 41 K. Gong, F. Du, Z. Xia, M. Durstock and L. Dai, *Science*, 2009, **323**, 760–764.
- 42 D. Yu, Q. Zhang and L. Dai, *J. Am. Chem. Soc.*, 2010, **132**, 15127–15129.
- 43 Z. Wang, R. Jia, J. Zheng, J. Zhao, L. Li, J. Song and Z. Zhu, *ACS Nano*, 2011, **5**, 1677–1684.